Marine Oil Slicks Quantification From L-band Dual-Polarization SAR Imagery

Olivier Boisot, Sébastien Angelliaume, and Charles-Antoine Guérin

***Abstract*— We show, using simple physical models, that a quantitative estimation of the volume fraction of marine oil slicks can be achieved from dual-polarization synthetic aperture radar (SAR) imagery. Volume fraction, which quantifies the proportion of seawater in oil in the case of a mixture, depends primarily on volume scattering mechanisms and is inferred from the polarization ratio in the L-band. A quantification algorithm is derived, namely, the volume fraction estimation algorithm that is applied to two experimental data sets acquired in the Mediterranean Sea during the POLLUPROOF'2015 exercise and in the North Sea during the NOFO'2015 experiment using the Office National d'Études et de Recherches Aérospatiales airborne L-band SETHI system. The resulting volume fraction maps of the quantification method are presented and discussed, opening new perspectives for marine oil slicks monitoring by means of dual-polarization SAR imagery.**

***Index Terms*— Complex effective permittivity, dual-polarization synthetic aperture radar (SAR), L-band, marine oil slick, ocean radar sensing, quantification, volume fraction.**

I. Introduction

AIRBORNE and spaceborne remote sensing sensors are commonly used by authorities and oil and gas companies to monitor hydrocarbons in the offshore domain [1]–[3]. The interest in remote sensing techniques lies not only in the global monitoring of the maritime environment to detect and track incidents or possible boat fuel releases but also in the identification of the natural occurrence of crude oils (seeps) on the ocean surface, testing the presence of mature source rock on the seafloor [4]. Today, state-of-the-art approaches for detecting oil slicks at sea are typically based on synthetic aperture radar (SAR) imagery [5]–[7], which is not impacted by weather conditions as the optical imagery.

Marine oil slicks can be found under two primary forms, namely, surfactant films and crude oil slicks. Surfactant (surface-active agents) films are thin surface films made of *amphiphilic* organic compounds, consisting of a *hydrophilic* head group and a *hydrophobic* tail, which arrange themselves as monomolecular films whose thickness is, typically, 2.4–2.7 nm [8]. Their occurrence has been observed for sea surface wind speed $u_{10} \leq 5$ ms^{-1} [9], otherwise, they are mixed and dissolved in the bulk water. When originating from natural sources, which is the most frequent case, they are referred to as *biogenic* or *natural* films. These films are mostly observed in coastal and upwelling zones where marine fauna and flora activity is intense. Surfactant films can also be observed from accidental vegetable oil spills [10], [11] or at the edge of crude oil slicks due to weathering processes.

Crude oil slicks (including mineral oils and refined product of crude oils) are organic compounds constituted of alkanes, cycloalkanes, and aromatics with the preferentially hydrophobic characteristic. When released at sea, crude oils are mixed with seawater under the action of wind and waves, resulting in a slick composed of a mixture of oil and water, such as emulsion, underneath an oil film. Oil and water emulsions are composed of small droplets of one medium in the background of the other, that is, water-in-oil (W/O) or oil-in-water (O/W) emulsions. The most frequently encountered offshore emulsions are the W/O case, but O/W emulsions can also be found [12]. Droplets' diameter of such emulsions is lower than 1 μm in the case of a fine emulsion, whereas larger than 1 μm in the case of coarse emulsions [12]. In the case of W/O emulsion, the water content is generally between 50% and 75% [13]. Crude oil slicks form thick layers at the sea surface ranging typically from micrometer to millimeter but can reach centimeter-range thickness in the case of fresh oil spill (accidents) and low sea state [8]. They originate mainly from anthropogenic sources such as oil rigs, ships, and so on but also from natural seeps.

The impact of monolayer surfactants on the sea surface has been well investigated since the 1960s. Various aspects have been addressed such as physicochemical approaches [14]–[16], experimental and laboratory studies [17]–[19], and the implications in remote sensing [20]–[24]. Even though the thickness of surfactant films is far smaller than that of crude oil slicks, their impact on the sea surface damping is of the same order of magnitude, which results in a damping of Bragg-wavelength capillary–gravity waves. Oil and seawater emulsions modify the dielectric properties of the remotely sensed surface, thus impacting the scattering coefficients of the scattering process. These two combined effects result in a global attenuation of the electromagnetic (EM) backscattered signal. As a result,

Manuscript received April 6, 2018; revised June 18, 2018, July 31, 2018, and August 29, 2018; accepted September 19, 2018. This work was supported by the Total (the French Petroleum Company) and Office National d'Études et de Recherches Aérospatiales (the French Aerospace Laboratory) through the New Advanced Observation Method Integration Project. *(Corresponding author: Olivier Boisot.)*

O. Boisot and S. Angelliaume are with the Département d'Électromagnétisme et Radar, ONERA, F-13661 Salon Cedex Air, France (e-mail: olivier.boisot@onera.fr).

C.-A. Guérin is with the Université de Toulon, Aix-Marseille Université, CNRS-INSU, IRD, Mediterranean Institute of Oceanography (MIO UM110), 83957 La Garde, France.

Color versions of one or more of the figures in this paper are available online at http://ieeexplore.ieee.org.

Digital Object Identifier 10.1109/TGRS.2018.2872080

TABLE I
EXAMPLES OF SEAWATER THERMOPHYSICAL PROPERTIES AS WELL AS OIL SLICK PARAMETERS AND W/O MIXTURE EFFECTIVE COMPLEX PERMITTIVITY AS FUNCTION OF THE FREQUENCY BAND

Frequency Band	seawater properties ($SST = 10°C$; $SAL = 35$ PSU)				crude oil slick (from [33])		W/O mixture
$[f_{EM}]$ (GHz)	ε_{sw}	η_{sw} [mPa.s]	ρ_{sw} [kg.m^{-3}]	σ_{sw} [mN.m^{-1}]	$\lvert E\rvert$ [mN.m^{-1}]	β [°]	ε_{eff} @ $f_v = 0.5$
L [1]	74.77+73.71i	1.397	1027	74.89	22.9	-165.5	23.19+18.83i
C [5]	66.45+36.78i						20.88+9.507i
X [10]	49.81+40.44i						16.65+10.65i

marine oil slicks appear as dark patches in the SAR images, compared to the surrounding sea surface.

Essential requirements for global monitoring of oil at sea and efficient clean-up operations are the identification of the impacted area as well as its characterization (nature of oil) and its quantification (volume of oil). Many methods have been proposed in the past decades for the detection of oils on the ocean surface, many of them relying on SAR data (see [23] and [24] for a review). The most relevant radar parameters for marine oil slicks detection have been recently identified in [25] together with the most appropriate imaging mode in the context of marine pollution detection. Different studies have concentrated their efforts to characterize and discriminate oil spills from *look-alike phenomena* [26], [27], while others have investigated the mixing of oil and seawater from SAR sensors [28]–[30]. Up to now, only an oil/seawater mixing classification has been proposed, namely, the *oil/seawater mixing index* M ($-1 \leq M \leq 1$) [28]. This index characterizes the oil and seawater mixing type by differentiating the origin of the attenuation of the backscattered signal in presence of an oil slick. Positive values indicate an attenuation mostly due to surface roughness damping from a surface film, whereas negative values indicate an attenuation mostly due to a modification of the relative complex permittivity from a mixture of oil and seawater. This index has been used later in [30] where a methodology has been proposed based on dual copolarized (HH and VV) SAR images to detect and quantify the relative concentration of pollutant on the ocean surface.

We present in this paper a novel methodology for the quantitative retrieval of the *volume fraction* (f_v) of an oil and seawater mixture. The volume fraction estimation (VFE) is mainly related to the effective complex permittivity of the underneath oil and seawater mixture and can be evaluated from the *polarization ratio* (PR) in the L-band together with the effective complex permittivity. The proposed methodology makes a combined utilization of models pertaining to the surface roughness, the complex permittivity, and the scattering process at the sea surface. These models are reviewed in Section II. In Section III, the quantification algorithm is introduced and its range of application discussed. The first application to experimental SAR data is presented in Section IV.

II. PHYSICAL MODELING

A. Sea Surface

1) Spectral Modeling of Sea Surface: One of the most popular sea surface wavenumber spectrum models today is the unified directional spectrum proposed by Elfouhaily *et al.* [31], which has been designed to address the complete range of wave scales and sea states. It combines various theoretical and experimental results in order to derive a directional sea wavenumber spectrum taking into account a wide range of sea wavelength, ranging from gravity to capillarity waves. The spreading function describing its azimuthal dependence is limited to the first even Fourier harmonic

$$\Psi(k, \phi_k) = \frac{\Psi_0(k)}{2\pi k}[1 + \Delta(k)\cos(2(\phi_k - \phi_w))] \tag{1}$$

where (k, ϕ_k) are the polar coordinates of the sea surface wavenumber, the function $\Delta(k)$ is defined as the ratio of the upwind/crosswind directional spectrum, and ϕ_w is the wind direction.

2) Seawater Complex Permittivity: One important descriptive parameter for seawater in presence of oil is the complex relative dielectric permittivity

$$\varepsilon = \varepsilon' + \mathrm{i}\varepsilon.'' \tag{2}$$

It is customary to refer to the real part ε' as the *relative permittivity* and to the imaginary part ε'' as the *loss factor*. Seawater is a dispersive medium with high values of relative permittivity and loss factor. A recent model, based on the classical *double-Debye dielectric model* and adjusted to microwave satellite data can be found in [32], and examples are provided in Table I.

3) Thermophysical Properties of Seawater: Thermophysical properties of seawater are quite similar to those of pure water. However, dissolved salt in water makes a difference that must be taken into account in modeling the interaction of seawater and oils mixture. A review of thermophysical properties has been provided by Sharqawy *et al.* [34] where many models have been updated. Examples can be found in Table I.

B. Impact of Oil at Sea

1) Sea Roughness Damping Model: It was the Italian physicist Marangoni [35] who first realized that wave damping from viscous surface films on seawater is due to the change in surface tension caused by waves motion. Later on, Cini and Lombardini [15] were the first to formalize the effect of resonance-type damping in the short-gravity waves region, also called as the *Marangoni effect*, from monomolecular surfactant films. A review of the damping effect can be found in [36]. Denoting Δ_{oil}, the viscous coefficient of the sea surface covered by a monomolecular surfactant film and Δ_{sw}, the film-free sea surface, the viscous damping ratio is [36]

$$y(k) = \frac{\Delta_{\mathrm{oil}}}{\Delta_{\mathrm{sw}}} = \frac{1 + X(\cos\beta - \sin\beta) + XY - Y\sin\beta}{1 + 2X(\cos\beta - \sin\beta) + 2X^2} \tag{3}$$

where

$$X = \frac{|E|k^2}{\sqrt{2\omega_{\mathrm{sw}}^3 \eta_{\mathrm{sw}} \rho_{\mathrm{sw}}}} \quad \text{and } Y = \frac{|E|k}{4\omega_{\mathrm{sw}}\eta_{\mathrm{sw}}} \tag{4}$$

TABLE II
SOME VALUES OF COMPLEX DILATATIONAL ELASTICITY MODULI OF CRUDE OILS [33]

Oil number	Oil origin	$\|E\|$ [mN.m^{-1}]	β [°]
1	West Africa	12.2	-166
2	West Africa	9.3	-161.1
3	North Sea	22.9	-165.5
4	North Sea	32.9	-166.5
5	France	14.4	-165.6

with $E = -|E|\exp(\mathrm{i}\beta)$ being the complex dilatational elasticity modulus of the oil film (with $|E|$ in [N.m^{-1}] and β the phase angle), k being the wavenumber of waves, $\omega_{\mathrm{sw}} = (gk + \sigma_{\mathrm{sw}}/\rho_{\mathrm{sw}}k^3)^{1/2}$ being the capillarity–gravity waves dispersion relationship, g being the gravity constant at the sea level, and η_{sw}, ρ_{sw}, and σ_{sw} being the dynamic viscosity, the volumetric mass, and the surface tension of seawater, respectively. Table II recaps some values of the complex dilatational modulus E, taken from [33], for some crude oils. Other examples, in the case of biogenic slicks, can be found in [36].

Further calculations of the damping ratio induced by a viscous surface film in the case of finite thickness film have been conducted by Jenkins and Jacobs [37]. It has been shown that (3) is the limiting case of a zero thickness film, holding for thickness film smaller than 0.1 mm in general. It also holds for surface layers smaller than 1 mm under the assumption that the kinematic viscosity ratio ($\nu_{\mathrm{oil}}/\nu_{\mathrm{sw}}$) remains smaller than 100 [37]. However, this last assumption is not verified for the majority of known oils, due to a very large variation of viscosity values from one oil to another [13]. Nevertheless, an oil layer at sea level is quickly spread and mixed by weathering processes such as natural wind stress and waves motion. One can thus assume that the condition of an oil layer smaller than 0.1 mm is satisfied in a majority of cases, except in the specific case of fresh release of crude oils by low sea state. Equation (3) of the viscous damping ratio can, therefore, be used for general marine oil slicks and not only for monolayer surfactants such as biogenic slicks.

The viscous damping ratio y can be related to the sea spectrum damping ratio D_Ψ if one assumes that surface films are partially dispersed by wind stress and waves motion, resulting in a partial film coverage of the surface. Introducing a *surface fraction* factor f_s to quantify the area covered by a film among the total sea surface area impacted by the slick ($0 \leq f_s \leq 1$), the sea spectrum damping ratio is given by [38]

$$D_\Psi(k) = \frac{\Psi_{\mathrm{sw}}(k)}{\Psi_{\mathrm{oil}}(k)} = \frac{1}{1 - f_s + f_s/y(k)} \tag{5}$$

with Ψ_{sw} standing for the film-free sea wavenumber spectrum and Ψ_{oil} the film-covered sea wavenumber spectrum.

2) Oil Complex Permittivity: Oils are dielectric media with low relative permittivity and very small loss factor. In the microwave range, going from L-band to X-band, oils are a quasi-nondispersive medium; their relative permittivity ranges from about 2.2 to 2.3 and their loss factor is about 0.01 [39], [40]. We will adopt the following value of the oil complex permittivity, which is valid in the frequency range 1–10 GHz:

$$\varepsilon_{\mathrm{oil}} \simeq 2.25 + 0.01\mathrm{i}. \tag{6}$$

3) Effective Complex Permittivity of a Mixture: Both W/O and O/W emulsions can be found at sea [12], so that inclusions and background environment can be inverted, with no *a priori* knowledge of the mixture type. In the case of homogeneous *spherical* inclusions (ε_i) in a homogeneous environment (ε_e) with a *volume fraction* $f_v = V_i/V_e$, the classical Bruggeman formula [41] is the most adapted as it does not assume one medium or the other to be the background environment. It provides an explicit formula for the *effective complex permittivity* of the mixture

$$\begin{cases} \varepsilon_{\mathrm{eff}} = \dfrac{1}{4}\{\varepsilon_e - (1-3f_v)(\varepsilon_i - \varepsilon_e) + \cdots \\ \qquad \sqrt{[\varepsilon_e - (1-3f_v)(\varepsilon_i - \varepsilon_e)]^2 + 8\varepsilon_i\varepsilon_e}\} \\ f_v = \dfrac{(\varepsilon_{\mathrm{eff}} - \varepsilon_e)(\varepsilon_i + 2\varepsilon_{\mathrm{eff}})}{3\varepsilon_{\mathrm{eff}}(\varepsilon_i - \varepsilon_e)} \end{cases}. \tag{7}$$

Examples of W/O mixture effective complex permittivity as function of the EM band are given in Table I.

C. Surface Scattering

1) Splitting Rule: In order to distinguish volume and surface scattering effects, Guérin and Sentenac [42] derived a so-called *splitting rule*:

The incoherent intensity of a composite medium with a rough interface is the sum of the incoherent intensity of a rough homogeneous surface with an effective permittivity and the incoherent intensity of the same composite medium below a flat interface. The coherent intensity is merely that of the rough effective homogeneous surface.

Thus, volume effects can be associated with the effective complex permittivity of the mixture in the water column and surface effects to the roughness of the surface, considering the effective complex permittivity of the homogeneous medium at the interface.

2) Universal Weighted Curvature Approximation: There exists a wealth of surface scattering models to describe the interaction of EM wave with the sea surface [43]. The key parameters for radar observation, which depend on the viewing angles (namely, the incidence angle θ and the azimuth angle ϕ) as well as the surface roughness, are the *normalized radar cross section* (NRCS, σ^0_{pp}) and the PR, among others

$$\mathrm{PR} = \frac{\sigma^0_{\mathrm{HH}}}{\sigma^0_{\mathrm{VV}}}, \quad 0 < PR \leq 1 \tag{8}$$

where σ^0_{HH} and σ^0_{VV} are the copolarized horizontal and vertical NRCSs, respectively. As usual, the choice of a model results from a tradeoff between simplicity and performance. Asymptotic surface scattering models, such as the classical *small perturbation method* [44], [45], the *Kirchhoff approximation* [46], or the first-order *small-slope approximation* (SSA) [47]–[49], can be used under some specific conditions (low incidence angles, small roughness, etc.) but predict a purely geometrical angular variation of the PR and thus cannot account for their roughness dependence. Nontrivial PRs and

a better reproduction of the azimuthal behavior of the NRCS can be obtained with the family of two-scale models, which account for the tilting effects of large-scale waves onto small ripples [45], [50], [51]. Improved scattering models can also be obtained with functional or perturbative expansions with respect to an elevation, a slope, or a curvature parameter such as the *second-order SSA* [48] or models taking explicitly into account the local surface curvature [52]–[58]. Among these models, which are more complex to use than the classical asymptotic models, we adopted one simple unifying model that has been found to address the variety of scales at the sea surface and to describe properly the roughness dependence of the PR while being well adapted to the inversion of oceanic parameters, namely the so-called *universal weighted curvature approximation* (UWCA), first introduced in [57]. This model depends only on the sensor viewing angles and the sea surface wavenumber spectrum. Its expression for the copolarized NRCS is given by

$$\sigma^0_{pp} = 4\pi\,|\mathbb{B}_{pp}|^2\Psi(\mathbf{Q_H}) + |\mathbb{K}|^2[I_s - 4\pi\,\Psi(\mathbf{Q_H})] \tag{9}$$

where

$$I_s = \frac{1}{\pi\,Q_z^2}\int_{\mathbb{R}^2} \mathrm{e}^{-\mathrm{i}\mathbf{Q_H}\cdot\mathbf{r}}\left[\mathrm{e}^{-Q_z^2[\rho(\mathbf{0})-\rho(\mathbf{r})]} - \mathrm{e}^{-Q_z^2\rho(\mathbf{0})}\right]d\mathbf{r} \tag{10}$$

is proportional to the classical Kirchhoff integral, $\mathbf{Q_H}$ and Q_z are the horizontal and vertical projections of the Ewald vector: $\mathbf{Q} = \mathbf{Q_H} + Q_z\hat{\mathbf{z}}$, ρ is the spatial autocorrelation function of the sea surface, and $\Psi(\mathbf{Q_H})$ is the sea wavenumber spectrum taken at the Bragg wavenumber

$$||\mathbf{Q_H}|| = 2K_0\sin\theta = K_B \tag{11}$$

with K_0 being the EM wavenumber. The expression of the Bragg ($\mathbb{B}_{pp}$) and Kirchhoff ($\mathbb{K}$) kernels can be found in [43]. In the following, we introduce the *relative roughness* coefficient Γ

$$\Gamma(\theta,\phi) = \frac{4\pi\,\Psi(\mathbf{Q_H})}{I_s} \tag{12}$$

which quantifies the proximity to a Bragg scattering mechanism. This coefficient varies from 0 (pure facet reflections) to 1 (pure Bragg resonance mechanisms). We may therefore rewrite (9)

$$\sigma^0_{pp} = I_s[\Gamma|\mathbb{B}_{pp}|^2 + (1-\Gamma)|\mathbb{K}|^2] \tag{13}$$

leading to the following expression for the PR (8):

$$\mathrm{PR} = \frac{\Gamma|\mathbb{B}_{\mathrm{HH}}|^2 + (1-\Gamma)|\mathbb{K}|^2}{\Gamma|\mathbb{B}_{\mathrm{VV}}|^2 + (1-\Gamma)|\mathbb{K}|^2} = \mathrm{PR}(\theta,\phi,\varepsilon). \tag{14}$$

In this form, the azimuthal variations of the PR are clearly controlled by the relative roughness Γ defined in (12).

III. Quantification Method

The developed quantification method aims at estimating the volume fraction f_v of an oil and seawater mixture, which quantifies the proportion of seawater in oil. The respective contributions of volume and surface modifications can be separated, owing to the aforementioned splitting rule. The estimation algorithm, referred to as the VFE algorithm, relies on the PR properties in the L-band and the comparison of the slick-impacted area with the surrounding slick-free seawater used as an absolute reference. In the case of SAR images with complete slick coverage, the method could still be applied using a sea surface wave spectrum model to estimate the slick-free seawater NRCS but would provide qualitative results only, due to the unknown actual roughness of the sea surface.

As seen in (14), the PR at a given angle of incidence depends essentially on the relative roughness coefficient of the surface (Γ) and the complex relative permittivity of the medium (ε). The different PRs, depending on the configuration of the composite medium can be summarized as

$$\begin{aligned}
\mathrm{PR_{sw}} &= \mathrm{PR}(\Gamma_{\mathrm{sw}},\varepsilon_{\mathrm{sw}})\\
\mathrm{PR_{film}} &= \mathrm{PR}(\Gamma_{\mathrm{film}},\varepsilon_{\mathrm{sw}})\\
\mathrm{PR_{mix}} &= \mathrm{PR}(\Gamma_{\mathrm{sw}},\varepsilon_{\mathrm{eff}})\\
\mathrm{PR_{slick}} &= \mathrm{PR}(\Gamma_{\mathrm{film}},\varepsilon_{\mathrm{eff}})
\end{aligned} \tag{15}$$

where the "sw," "film," "mix," and "slick" subscripts stand for, respectively, the pure seawater, the pure viscous surface film, the pure W/O mixture, and oil slick (surface film + mixture) case. $\varepsilon_{\mathrm{eff}}$ is the effective complex permittivity of a W/O mixture. We expect the PR of film-covered areas ($\mathrm{PR_{film}}$) to depend explicitly on the underneath seawater complex permittivity due to the very small thickness of those surface films (from nanometer to millimeter, which is small compared to the penetration depth of the microwaves in pure oil [25]). Note also, the assumption regarding the PR of a W/O mixture ($\mathrm{PR_{mix}}$) is not completely true as an emulsion can have some damping effects on the sea roughness. However, as measured in [33], a fresh release of a pure W/O emulsion in seawater has a quasi-negligible viscous damping effect. Stronger viscous damping effects originate from the formation of a pure viscous film above the sea surface during weathering processes, resulting in oil slick.

Sea roughness damping by a surface film tends to decrease the PR, while on the contrary, a W/O mixture tends to increase it [25]. However, in the L-band, the former effect is negligible since the PR is dominated by the Bragg mechanism at a resonant wavelength which is little affected by the small-scale damping process. This is illustrated in Fig. 1 where calculations of the PR have been carried out in the upwind direction with the UWCA scattering model ((14)) and an Elfouhaily spectrum for a wind speed $u_{10} = 7\ \mathrm{ms}^{-1}$. In both X-band and L-band, the W/O mixture has a significant impact on the PR, while a surface viscous film only affects the X-band. Hence, the L-band relative roughness parameter of the surface film can be assumed unchanged with respect to its seawater counterpart

$$\Gamma_{\mathrm{film}} \simeq \Gamma_{\mathrm{sw}} \tag{16}$$

and the same holds for the corresponding PRs

$$\mathrm{PR_{slick}} \simeq \mathrm{PR}(\Gamma_{\mathrm{sw}},\varepsilon_{\mathrm{eff}}) = \mathrm{PR_{mix}}. \tag{17}$$

This shows that volume scattering taken into account by the effective complex permittivity has the dominant impact on the PR in the L-band while roughness damping effects are negligible. In the case of a seawater area impacted by a pure viscous surface film, the observed PR in the L-band ($\mathrm{PR_{film}}$)

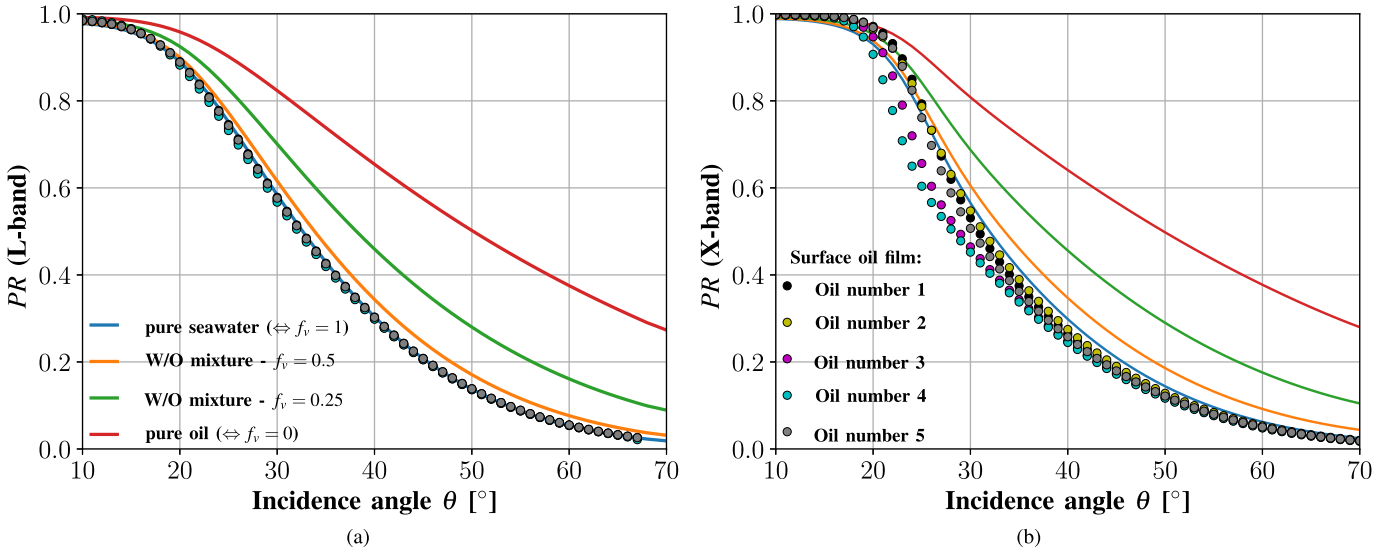

Fig. 1. PR as a function of the incidence angle in (a) L-band (1 GHz) and (b) X-band (10 GHz) for different types of surface: pure sea water (blue solid line), W/O mixtures (orange solid lines and green lines), and pure oil (red line). The calculation has been performed in the upwind direction with the UWCA scattering model using an Elfouhaily spectrum with wind speed $u_{10} = 7$ ms^{-1}. Colored dots depict the case of a dampened sea roughness induced by viscous surface oil films above the sea surface for a surface fraction of 1 and different values of complex dilatational modulus E, whose corresponding oil numbers are taken from Table II. In (a) L-band, all colored dots are superimposed. The seawater properties have been calculated for SST= 10°C and SAL= 35 PSU and can be found in Table I.

will thus appear similar to that of the surrounding seawater area ($\mathrm{PR_{sw}}$). An illustration of this phenomenon can be seen in [25, Fig. 13(d)] for real L-band SAR images recorded during the POLLUPROOF'2015 exercise developed later in this paper (see Section IV-A). With the use of L-band copolarized SAR data, the VFE algorithm runs as follows.

1) Estimation of the seawater complex permittivity ($\varepsilon_{\mathrm{sw}}$) from external data of sea surface temperature (SST) and salinity (SAL).
2) Estimation of the mean seawater relative roughness parameter (Γ_{sw}) from the mean seawater PR ($\mathrm{PR_{sw}}$) and the seawater complex permittivity ($\varepsilon_{\mathrm{sw}}$) on the largest available area, as a function of the sensor incidence angle

$$\Gamma_{\mathrm{sw}} = \left[1 + \frac{\mathrm{PR_{sw}}|\mathbb{B}_{\mathrm{HH}}(\varepsilon_{\mathrm{sw}})|^2 - |\mathbb{B}_{\mathrm{VV}}(\varepsilon_{\mathrm{sw}})|^2}{|\mathbb{K}(\varepsilon_{\mathrm{sw}})|^2(1-\mathrm{PR_{sw}})}\right]^{-1}. \tag{18}$$

3) Joint estimation of the effective complex permittivity ($\varepsilon_{\mathrm{eff}}$) and volume fraction ($f_v$) of the W/O mixture by solving the system

$$\begin{cases} \mathrm{PR}[\Gamma_{\mathrm{sw}}, \varepsilon_{\mathrm{eff}}] = \mathrm{PR_{data}} \\ \mathrm{Re}[\varepsilon_{\mathrm{eff}}] = \mathrm{Re}\left[\varepsilon_{\mathrm{eff}}^{\mathrm{Brug}}(\varepsilon_{\mathrm{sw}}, \varepsilon_{\mathrm{oil}}, f_v)\right] \\ \mathrm{Im}[\varepsilon_{\mathrm{eff}}] = \mathrm{Im}\left[\varepsilon_{\mathrm{eff}}^{\mathrm{Brug}}(\varepsilon_{\mathrm{sw}}, \varepsilon_{\mathrm{oil}}, f_v)\right] \end{cases} \tag{19}$$

where the effective complex permittivity used in the first line of (19) is constrained by the mixing rule of Bruggeman (7). This leads to a nonlinear system of three equations with three unknown parameters, which can be solved numerically with classical solvers. The solution is unique in view of the monotonic behavior of $\mathrm{PR}[\varepsilon_{\mathrm{eff}}]$, $\mathrm{Re}[\varepsilon_{\mathrm{eff}}^{\mathrm{Brug}}(f_v)]$, and $\mathrm{Im}[\varepsilon_{\mathrm{eff}}^{\mathrm{Brug}}(f_v)]$.

IV. Application to Experimental Data

A. Data Sets Presentation

The methodology presented in this paper has been applied to experimental SAR data collected with SETHI (the airborne remote sensing system developed by Office National d'Études et de Recherches Aérospatiales (ONERA) [59]) during two offshore oil-on-water exercises: POLLUPROOF'2015 and NOFO'2015.

The POLLUPROOF'2015 experiment (May 18 and 22, 2015) was conducted over the Mediterranean Sea (off the French coast, near 42°45.5' N, 5°48.5'E) and focused on the release and subsequent observation of several *hazardous and noxious substances* (HNSs). The main goal of this experiment was to establish a procedure for collecting evidence of illegal marine pollution by HNS from airborne sensors [30]. In the following, we will focus on the May 22, 2015 exercise where 1 m^3 of rapeseed oil (colza oil) and 1 m^3 of *fatty acid Methyl esters* (FAME, biofuel directly added in conventional fuels) were released at sea within a small time lag (see Table III). Rapeseed oil is classically used to simulate biogenic films on the sea surface and has already been imaged by SAR sensors [26], [60], [61], whereas FAME forms a cloud of microdroplets in the water column [30].

The NOFO'2015 experiment (June 8–14, 2015) is an oil spill cleanup exercise managed by the Norwegian Clean Seas Association for Operating Companies (NOFO). It was carried out in the North Sea (230-km NorthWest of Stavanger, Norway) within 10 Nautical Miles of position (59° 59′N, 02° 27′E). In the following, we will focus on the June 9, 2015 exercise during which the MOS Sweeper mechanical recovery boom [62] was tested at sea [25]. For this experiment, the released product was an emulsion of water in mineral oil with a water content of 60%. It consisted of a mixture of

TABLE III
ENVIRONMENTAL CONDITIONS AND PROPERTIES OF RELEASED SUBSTANCE

Experiment	Time of release (UTC)	Amount of release [m^3]	Released substance	Time of imaging (UTC)	Wind speed (10m) u_{10} [$m.s^{-1}$]	Wind direction (from) ϕ_w [°]	Radar look direction ϕ [°]	SST^a [°C]	SAL^a [PSU]
POLLU-PROOF	15:01-15:28 15:24-15:40	1	Rapeseed oil FAME	16:07	8.2	270	181	15.1	38.08
NOFO	06:30-08:00	45	Mineral oil	10:01	5.1	270	22	9.49	35.16

water, Oseberg crude oil, and a small addition of IFO 380 (intermediate fuel oil or marine diesel oil, with a viscosity of 380 $mm^2.s^{-1}$). For the trial, 45 m^3 of emulsion was discharged at sea. Assuming the entire volume of hydrocarbon was spread on the surface, the upper limit of the average thickness of the slick is about 1 μm [25].

Meteorological information was obtained from Météo-France, the French National Meteorological Center (POLLUPROOF'2015), and the Norwegian Meteorological Institute (NOFO'2015), while sea surface thermophysical characteristics were obtained from Copernicus Marine website (see Table III).

During both exercises, quadpolarimetric SAR data were collected with SETHI at the L-band with a range resolution of 1 m (bandwidth from 1.25 to 1.4 GHz). Images were processed with an azimuth (along track) resolution equal to the range resolution. The imaged area was about 9.2 km in azimuth and 1.1 km in range, with incidence angles spanning from 34° to 52°. The L-band SAR sensor that operated onboard SETHI is characterized by a very low instrument noise floor, allowing a sufficiently high *signal-to-noise ratio* (SNR) over both slick-free and slick-covered areas for valid analysis of surface characteristics.

The SNR is a crucial parameter in the context of marine oil slicks sensing with SAR and its impact must be carefully taken into account. As a matter of fact, the copolarized coherency has been claimed to decrease rapidly over slick-covered surface [24] but it was later suggested in [61] and demonstrated in [25] that this is mainly due to instrumental noise decorrelation. However, providing a sufficiently high SNR, it has been shown that the copolarized coherency parameter is not impacted by oil slicks [25], [29] and is, therefore, a useful parameter to eliminate ships and/or SAR processing artifacts, as was done with the present data sets.

For the SETHI instrument, the noise equivalent sigma zero (NESZ) estimated using the method proposed in [63] is very low, ranging from about -53.5 to -51 dBm^2/m^2 (see Fig. 2). High-resolution VV intensity images collected by SETHI during the two experiments are shown in Fig. 3. In the following, the range axis of images and maps has been dilated compared to the azimuth axis for clarity. Fig. 3(a) depicts the image acquired during the POLLUPROOF'2015 experiment in which the two successive spills are marked off by a yellow ellipse for the rapeseed oil and a red ellipse for the FAME. In between, a mixture of both products is formed and delineated by a blue ellipse [30]. Fig. 3(b) depicts the image acquired during the NOFO'2015 exercise where a feathered structure along the front of the slick and a smooth edge on its backside is observed, which is consistent with the wind direction (green arrow). The crossing of the MOS Sweeper mechanical recovery boom through the slick appears to leave behind a relatively clean sea surface (magenta arrow), and a wake is visible behind the crossing of a ship through the slick (cyan arrow).

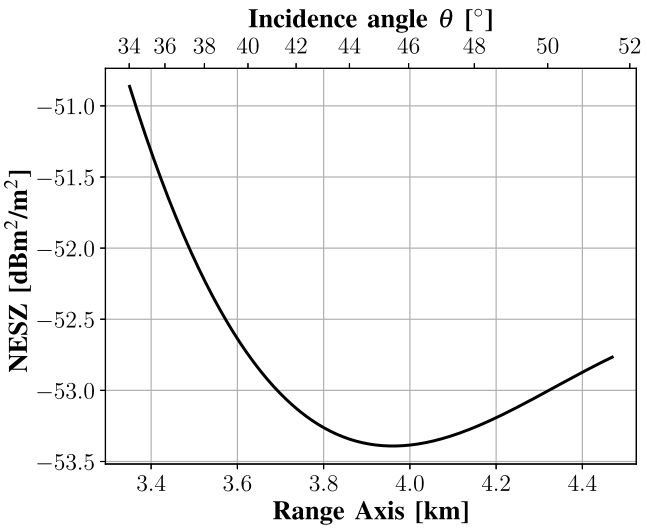

Fig. 2. SETHI L-band instrument noise floor (NESZ) as function of the radar range and sensor incidence angle for POLLUPROOF'2015 and NOFO'2015 experiments.

B. Results of the Quantification Method

The VFE algorithm was applied on both data sets presented in Section IV-A. Following the steps described in Section III, the seawater complex permittivity was estimated from the environmental conditions in Table III and from the central frequency of the SETHI system ($f_{\mathrm{EM}} = 1.325$ GHz) for both experiments

$$\begin{aligned} \text{POLLUPROOF'2015:}\varepsilon_{\mathrm{sw}} &\simeq 72.26 + 68.71\mathrm{i} \\ \text{NOFO'2015:}\varepsilon_{\mathrm{sw}} &\simeq 74.59 + 58.26\mathrm{i}. \end{aligned} \tag{20}$$

The reference PR of seawater ($\mathrm{PR_{sw}}$) was estimated by means of a slick-free detection mask and averaged over the maximum of available azimuth pixels. The slick detection mask was estimated by thresholding the *normalized polarization difference* (see [30] for a more detailed description) allowing to separate slick-free and slick-impacted areas. A morphological image processing method (binary opening: binary erosion followed by binary dilation) was applied on the mask in order to remove the last isolated points. The resulting PRs are shown in Fig. 4(a) as a function of the

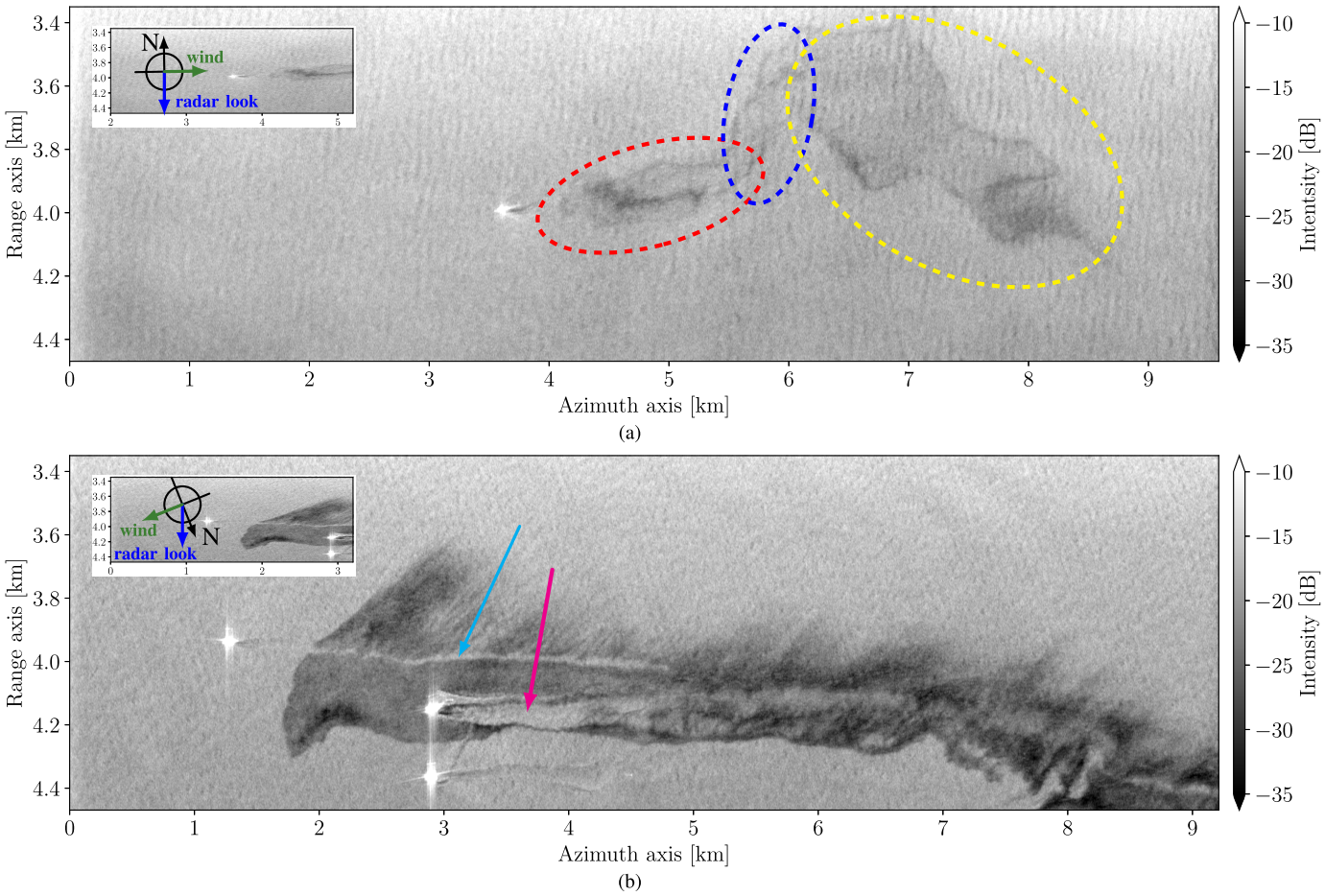

Fig. 3. L-band VV-polarization intensity images recorded during the (a) POLLUPROOF'2015 and (b) NOFO'2015 experiments. A 7 × 7 multilook processing has been applied. Thumbnails of corresponding images in an orthonormal basis are superimposed showing the geographical North (black arrow), the radar look direction (blue arrow), and the wind blowing direction (green arrow). Yellow and red ellipses: successive spills of rapeseed oil and FAME, respectively. In between, a mixture of both products is formed and delimited by a blue ellipse. Magenta and cyan arrows: relatively clean sea left behind the MOS Sweeper mechanical recovery boom and the wake left behind the crossing of a ship through the slick, respectively.

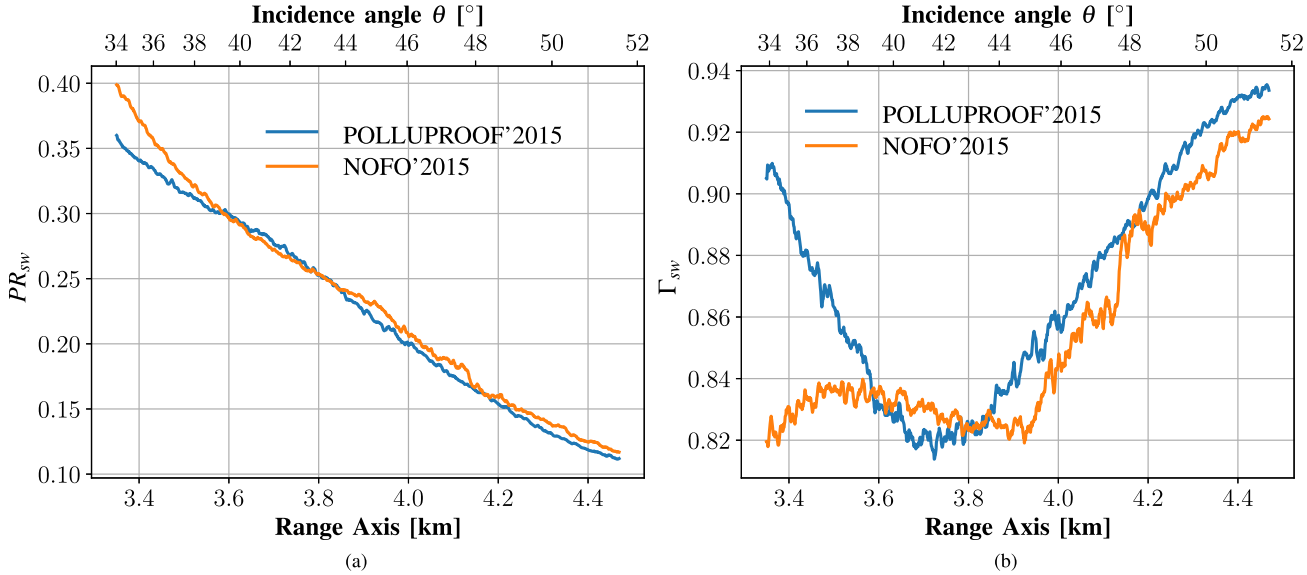

Fig. 4. (a) Estimated mean PR on seawater from detection mask and (b) corresponding relative roughness parameter on seawater from POLLUPROOF'2015 (blue curves) and NOFO'2015 (orange curves) L-band SETHI data (see Fig. 3).

radar range. The corresponding relative roughness parameters on seawater (Γ_{sw}) have been estimated through (18) and are depicted in Fig. 4(b).

The different shapes of Γ_{sw} parameters [Fig. 4(b)] depend directly on the different shapes of the corresponding PRs [Fig. 4(a)], which themselves depend on the acquisition

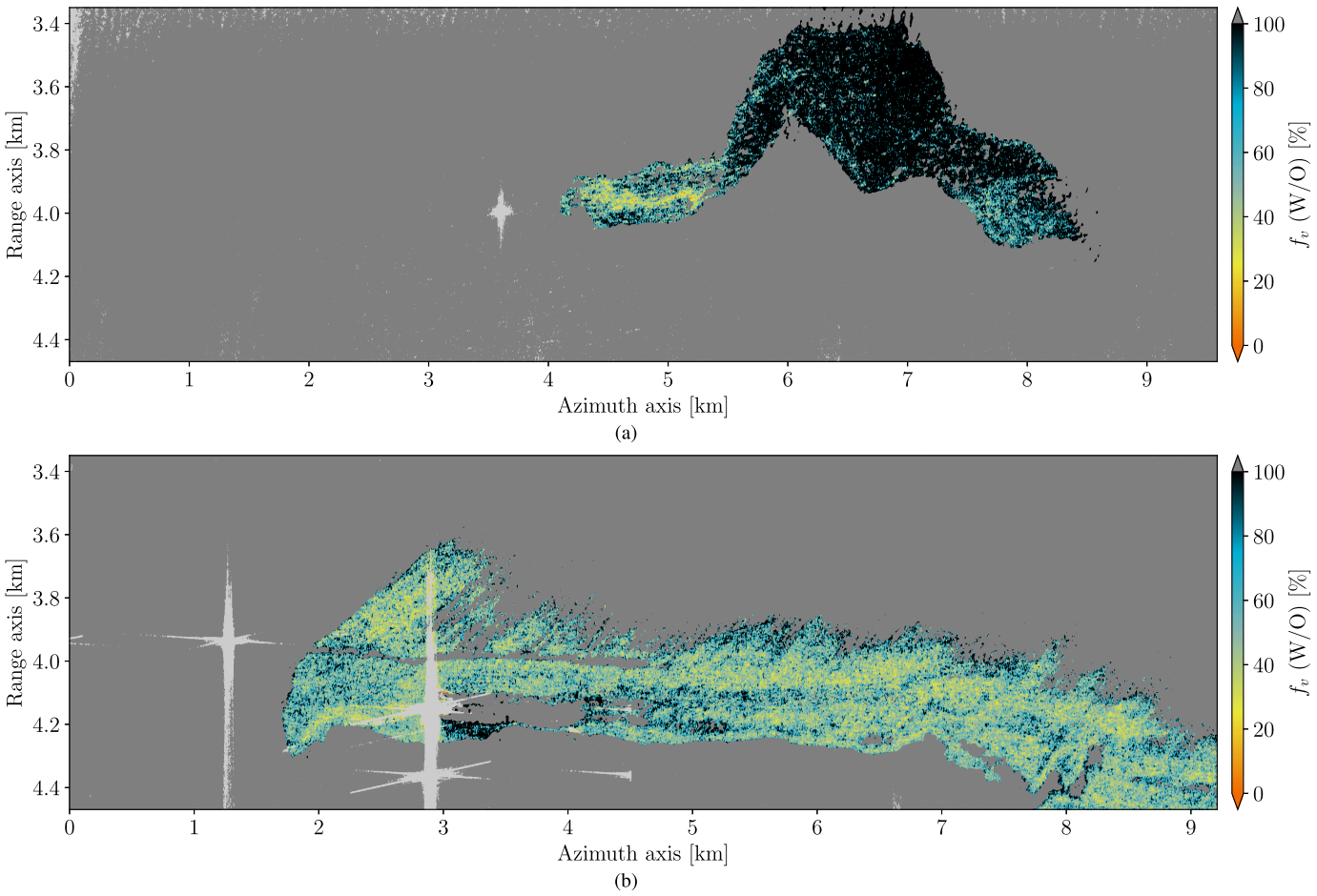

Fig. 5. Resulting W/O volume fraction maps from VFE algorithm applied to (a) POLLUPROOF'2015 and (b) NOFO'2015 L-band SETHI data (see Fig. 3). Dark gray area: slick detection mask. Light gray area: removal of ships and SAR processing artifacts.

geometry and sea state. The seawater PRs are found of the same order of magnitude as the predicted one in Fig. 1(a), ranging from about 0.35 to 0.4 in the near range ($\theta = 34°$) to about 0.12 in the far range ($\theta = 52°$). A small inflection of the PR is observed at about 3.7 and 3.9 km in range for the POLLUPROOF'2015 and NOFO'2015 experiments, correspondingly. This effect on the PR is assumed to come from the asymmetrical nature of the observed sea surface, as could be modeled qualitatively by adding a small percentage of asymmetrical *wedges* to the sea surface slope distribution [64]. The different locations of the inflection originate from the slightly different azimuth look directions and the different sea states between the two experiments. This inflection is reproduced on the relative roughness parameter Γ_{sw} [Fig. 4(b)] as a dip around the same range values. Nevertheless, the high value of the relative roughness parameter ($\Gamma_{\text{sw}} > 0.8$), which is a measure of the deviation from the first-order Bragg scattering mechanisms, ensures that the Bragg scattering is the dominant mechanism and validates the assumption made in (16) and (17), thus ensuring the enforceability of the VFE algorithm.

The numerical inversion of both the effective complex permittivity (ε_{eff}) and the W/O volume fraction (f_v) has been performed by solving system (19) pixel by pixel on the entire image (avoiding pure seawater areas through the detection mask). The numerical inversion algorithm has been written in Python 3 and executed on the ONERA computational server THOR equipped with 4× Intel Xeon E7-8867 V3 at 2.50 GHz and 16 cores, for a total of 64 available computational cores. Parallelization of the code has improved the computation time from about 30 h to about 25 min on this server, in the NOFO'2015 data case. The resulting W/O volume fraction maps and real part of the effective complex permittivity of the two experiments are pictured in Fig. 5. Dark gray area represents the slick detection mask, and light gray area represents the ships and SAR processing artifacts removal by means of the copolarized coherency.

Fig. 5(a) depicts the resulting W/O volume fraction map estimated from the POLLUPROOF'2015 data. The left part of the slick (FAME release) shows a relatively low W/O volume fraction (yellow color, elevated oil concentration), while the rest of the slick (rapeseed oil release) exhibits a W/O volume fraction close to 1 (black color, very low oil concentration) indicating quasi-nonmixing of rapeseed oil with seawater, which is consistent with the biogenic behavior of the rapeseed oil. Nevertheless, the very right part of the slick (the beginning of the rapeseed oil release) shows shaded values of W/O volume fraction (blue color), indicating the onset

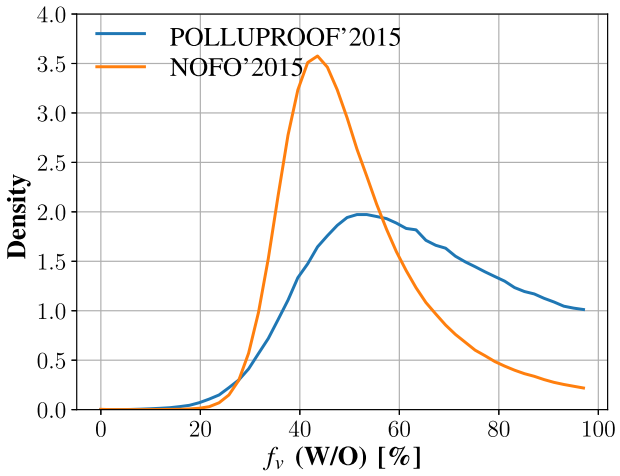

Fig. 6. Density functions of estimated W/O volume fractions depicted on Fig. 5.

of mixing of the rapeseed oil with seawater, likely due to weathering processes induced by wind. Indeed, during the POLLUPROOF'2015 experiment, an 8.2 ms^{-1} wind speed was recorded (see Table III) which is greater than 5 ms^{-1}, the observed upper limit of existence of biogenic slick related to wind speed [9]. Thus, indicating that the beginning of the rapeseed oil release is probably being mixed and dissolved in the bulk water. This W/O volume fraction map can be compared to the M_α map pictured in [30, Fig. 10(b)] calculated on the same data set. Indeed, the estimation of the mixing index M introduced in [28], characterizing the origin of the attenuation of the backscattered signal by the presence of a slick, depends on the difference between two parameters

$$M = M_W - M_\alpha \tag{21}$$

where the *normalized damping factor* $M_W (0 \leq M_W \leq 1)$ is a measure of the surface roughness damping by the slick (0 indicates no damping and 1 denotes a total damping) and the *normalized power attenuation factor* $M_\alpha (0 \leq M_\alpha \leq 1)$ is a measure of the attenuation of the backscattered signal due to a modification of the effective complex permittivity from a mixture (0 indicates no attenuation and 1 denotes a total attenuation) [28]. The areas of the impacted backscattered signal from a W/O mixture calculated with the M_α parameter depicted on [30, Fig. 10(b)] are very consistent with the values of the estimated W/O volume fraction shown in Fig. 5(a), with the difference that here, a quantitative proportion of W/O is provided.

Fig. 5(b) depicts the resulting W/O volume fraction map estimated from the NOFO'2015 data. This map shows an important variation of W/O volume fraction within the entire slick. A W/O volume fraction close to 1 (null oil concentration) is seen right behind the MOS Sweeper mechanical recovery boom (around range 4.2 km and between 3 and 4.5 km in azimuth), whereas a more graduated variation is observed far behind it, showing the reforming of the slick due to weathering processes. An increasing value of W/O volume fraction is seen in the drag of the slick (top of the image, from yellow to black color) showing a decrease in the oil concentration originating from weathering processes.

The resulting W/O volume fraction density functions calculated in Fig. 5 and plotted in Fig. 6 show a non-Gaussian distribution of W/O volume fractions within both slicks. The density function calculated with the NOFO'2015 data (orange curve) has a narrow peak around about 43%, whereas the density function calculated with the POLLUPROOF'2015 data (blue curve) is much wider. In both cases, the distributions decrease for low value and vanish for W/O volume fractions lower than about 20%. At large values, the NOFO'2015 distribution slightly decreases to the pure seawater case ($f_v = 100\%$), while on the contrary, the POLLUPROOF'2015 distribution remains elevated in the pure seawater case, which is consistent with the presence of the rapeseed oil film in the slick.

V. Conclusion

We presented a marine oil slicks quantification method to estimate the volume fraction, together with the complex effective permittivity, of a W/O mixture from the L-band dual-polarization SAR imagery. The quantification method is based on the physical modeling of both oil/seawater and EM waves/sea surface interactions. The UWCA scattering model was chosen as a good tradeoff between a relevant description of the polarimetric parameters and simple and versatile formulation well adapted to the inversion of oceanic features. An inversion algorithm has been derived, namely, the VFE algorithm, for the study of volume scattering effects. It uses the L-band PR properties and allows one to estimate the effective complex permittivity of the observed surface in addition to the W/O volume fraction. The enforceability of the algorithm is ensured through the high value of the relative roughness parameter ($\Gamma > 0.8$), showing that Bragg scattering is the dominant mechanism. Therefore, this algorithm can solely be applied to the L-band SAR data that also have very low noise level. These requirements are reached by actual airborne sensors such as the American Uninhabited Aerial Vehicle Synthetic Aperture Radar or the French SETHI systems but the use with satellite data, such as the Japanese L-band Advanced Land Observing Satellite system, would be limited by the instrument noise level. A first application of the VFE algorithm has been made to the L-band dual-polarized experimental data recorded during the POLLUPROOF'2015 and NOFO'2015 experiments with the ONERA airborne SETHI system, leading to a very consistent map of the W/O volume fraction. This kind of oil concentration map could be used in different manners and for different field of applications. For instance, in environmental monitoring, it could be used to concentrate cleaning efforts to the most oil-concentrated area in the case of accidental oil spill. Oil concentration map could also be used for temporal monitoring of oil concentration in the survey of natural oil seeps or other marine oil slicks.

Acknowledgment

The authors would like to thank all people involved in this project, and especially P.-Y. Foucher, V. Miegebielle, and D. Dubucq for supporting this paper. They would also like

to thank ONERA's Engineer J. Martinot-Lagarde for his very useful help in Python code parallelization, and the NOFO (Norwegian Clean Seas Association for Operating Companies) for allowing them to participate in the oil-on-water exercise, which was carried out during the period June 8–14, 2015.

REFERENCES

[1] I. Leifer *et al.*, "State of the art satellite and airborne marine oil spill remote sensing: Application to the BP *Deepwater Horizon* oil spill," *Remote Sens. Environ.*, vol. 124, pp. 185–209, Sep. 2012. [Online]. Available: http://www.sciencedirect.com/science/article/pii/S0034425712001563

[2] C. Brekke and A. H. S. Solberg, "Oil spill detection by satellite remote sensing," *Remote Sens. Environ.*, vol. 95, no. 1, pp. 1–13, Mar. 2005. [Online]. Available: http://www.sciencedirect.com/science/article/pii/S0034425704003724

[3] M. Fingas and C. Brown, "Review of oil spill remote sensing," *Mar. Pollut. Bull.*, vol. 83, no. 1, pp. 9–23, 2014. [Online]. Available: http://www.sciencedirect.com/science/article/pii/S0025326X14002021

[4] R. Jatiault, D. Dhont, L. Loncke, and D. Dubucq, "Monitoring of natural oil seepage in the lower congo basin using SAR observations," *Remote Sens. Environ.*, vol. 191, pp. 258–272, Mar. 2017. [Online]. Available: http://www.sciencedirect.com/science/article/pii/S0034425717300445

[5] M. Gade and W. Alpers, "Using ERS-2 SAR images for routine observation of marine pollution in European coastal waters," *Sci. Total Environ.*, vols. 237–238, pp. 441–448, Sep. 1999. [Online]. Available: http://www.sciencedirect.com/science/article/pii/S0048969799001564

[6] F. Girard-Ardhuin, G. Mercier, F. Collard, and R. Garello, "Operational oil-slick characterization by SAR imagery and synergistic data," *IEEE J. Ocean. Eng.*, vol. 30, no. 3, pp. 487–495, Jul. 2005.

[7] O. Garcia-Pineda, B. Zimmer, M. Howard, W. Pichel, X. Li, and I. R. MacDonald, "Using SAR images to delineate ocean oil slicks with a texture-classifying neural network algorithm (TCNNA)," *Can. J. Remote Sens.*, vol. 35, no. 5, pp. 411–421, Oct. 2009, doi: 10.5589/m09-035.

[8] M. Gade, H. Hühnerfuss, and G. M. Korenowski, *Marine Surface Films: Chemical Characteristics, Influence on Air-Sea Interactions and Remote Sensing*. Berlin, Germany: Springer, 2006, doi: 10.1007/3-540-33271-5.

[9] J.-C. Romano, "Sea-surface slick occurrence in the open sea (Mediterranean, Red Sea, Indian Ocean) in relation to wind speed," *Deep Sea Res. I, Oceanograph. Res. Papers*, vol. 43, no. 4, pp. 411–423, 1996. [Online]. Available: http://www.sciencedirect.com/science/article/pii/0967063796000246

[10] S. M. Mudge, M. A. Salgado, and J. East, "Preliminary investigations into sunflower oil contamination following the wreck of the M.V. *Kimya*," *Mar. Pollut. Bull.*, vol. 26, no. 1, pp. 40–44, 1993. [Online]. Available: http://www.sciencedirect.com/science/article/pii/0025326X9390596C

[11] S. M. Mudge, "Deleterious effects from accidental spillages of vegetable oils," *Spill Sci. Technol. Bull.*, vol. 2, nos. 2–3, pp. 187–191, 1995. [Online]. Available: http://www.sciencedirect.com/science/article/pii/S1353256196000199

[12] R. Pal, "Effect of droplet size on the rheology of emulsions," *AIChE J.*, vol. 42, no. 11, pp. 3181–3190, 1996, doi: 10.1002/aic.690421119.

[13] M. Fingas and B. Fieldhouse, "Studies on water-in-oil products from crude oils and petroleum products," *Mar. Pollut. Bull.*, vol. 64, no. 2, pp. 272–283, 2012. [Online]. Available: http://www.sciencedirect.com/science/article/pii/S0025326X11006114

[14] V. G. Levich, *Physicochemical Hydrodynamics*. Englewood Cliffs, NJ, USA: Prentice-Hall, 1962.

[15] R. Cini and P. P. Lombardini, "Damping effect of monolayers on surface wave motion in a liquid," *J. Colloid Interface Sci.*, vol. 65, no. 2, pp. 387–389, 1978. [Online]. Available: http://www.sciencedirect.com/science/article/pii/0021979778901704

[16] J. Lucassen, "Effect of surface-active material on the damping of gravity waves: A reappraisal," *J. Colloid Interface Sci.*, vol. 85, no. 1, pp. 52–58, 1982. [Online]. Available: http://www.sciencedirect.com/science/article/pii/002197978290234X

[17] S. A. Ermakov, A. M. Zujkova, A. R. Panchenko, S. G. Salashin, T. G. Talipova, and V. I. Titov, "Surface film effect on short wind waves," *Dyn. Atmos. Oceans*, vol. 10, no. 1, pp. 31–50, 1986. [Online]. Available: http://www.sciencedirect.com/science/article/pii/0377026586900084

[18] H. Hühnerfuss *et al.*, "Natural and man-made sea slicks in the North Sea investigated by a helicopter-borne 5-frequency radar scatterometer," *Int. J. Remote Sens.*, vol. 17, no. 8, pp. 1567–1582, 1996, doi: 10.1080/01431169608945364.

[19] M. Gade, W. Alpers, H. Hühnerfuss, and P. A. Lange, "Wind wave tank measurements of wave damping and radar cross sections in the presence of monomolecular surface films," *J. Geophys. Res., Oceans*, vol. 103, no. C2, pp. 3167–3178, 1998, doi: 10.1029/97JC01578.

[20] W. Alpers and H. Hühnerfuss, "Radar signatures of oil films floating on the sea surface and the marangoni effect," *J. Geophys. Res., Oceans*, vol. 93, no. C4, pp. 3642–3648, 1988, doi: 10.1029/JC093iC04p03642.

[21] V. Wismann, M. Gade, W. Alpers, and H. Hühnerfuss, "Radar signatures of marine mineral oil spills measured by an airborne multi-frequency radar," *Int. J. Remote Sens.*, vol. 19, no. 18, pp. 3607–3623, 1998, doi: 10.1080/014311698213849.

[22] M. Gade, W. Alpers, H. Hühnerfuss, V. R. Wismann, and P. A. Lange, "On the reduction of the radar backscatter by oceanic surface films: Scatterometer measurements and their theoretical interpretation," *Remote Sens. Environ.*, vol. 66, no. 1, pp. 52–70, 1998. [Online]. Available: http://www.sciencedirect.com/science/article/pii/S0034425798000340

[23] A. H. S. Solberg, "Remote sensing of ocean oil-spill pollution," *Proc. IEEE*, vol. 100, no. 10, pp. 2931–2945, Oct. 2012.

[24] M. Migliaccio, F. Nunziata, and A. Buono, "SAR polarimetry for sea oil slick observation," *Int. J. Remote Sens.*, vol. 36, no. 12, pp. 3243–3273, 2015, doi: 10.1080/01431161.2015.1057301.

[25] S. Angelliaume *et al.*, "SAR imagery for detecting sea surface slicks: Performance assessment of polarization-dependent parameters," *IEEE Trans. Geosci. Remote Sens.*, vol. 56, no. 8, pp. 4237–4257, Aug. 2018.

[26] S. Skrunes, C. Brekke, and T. Eltoft, "Characterization of marine surface slicks by radarsat-2 multipolarization features," *IEEE Trans. Geosci. Remote Sens.*, vol. 52, no. 9, pp. 5302–5319, Sep. 2014.

[27] S. Skrunes, C. Brekke, T. Eltoft, and V. Kudryavtsev, "Comparing near-coincident C- and X-band SAR acquisitions of marine oil spills," *IEEE Trans. Geosci. Remote Sens.*, vol. 53, no. 4, pp. 1958–1975, Apr. 2015.

[28] B. Minchew, "Determining the mixing of oil and sea water using polarimetric synthetic aperture radar," *Geophys. Res. Lett.*, vol. 39, no. 16, 2012, doi: 10.1029/2012GL052304.

[29] B. Minchew, C. E. Jones, and B. Holt, "Polarimetric analysis of backscatter from the Deepwater Horizon oil spill using L-band synthetic aperture radar," *IEEE Trans. Geosci. Remote Sens.*, vol. 50, no. 10, pp. 3812–3830, Oct. 2012.

[30] S. Angelliaume, B. Minchew, S. Chataing, P. Martineau, and V. Miegebielle, "Multifrequency radar imagery and characterization of hazardous and noxious substances at sea," *IEEE Trans. Geosci. Remote Sens.*, vol. 55, no. 5, pp. 3051–3066, May 2017.

[31] T. Elfouhaily, B. Chapron, K. Katsaros, and D. Vandemark, "A unified directional spectrum for long and short wind-driven waves," *J. Geophys. Res.*, vol. 102, no. C7, pp. 15781–15796, 1997.

[32] T. Meissner and F. J. Wentz, "The complex dielectric constant of pure and sea water from microwave satellite observations," *IEEE Trans. Geosci. Remote Sens.*, vol. 42, no. 9, pp. 1836–1849, Sep. 2004.

[33] N. Aske, R. Orr, and J. Sjöblom, "Dilatational elasticity moduli of water–crude oil interfaces using the oscillating pendant drop," *J. Dispersion Sci. Technol.*, vol. 23, no. 6, pp. 809–825, 2002, doi: 10.1081/DIS-120015978.

[34] M. H. Sharqawy, J. H. V. Lienhard, and S. M. Zubair, "Thermophysical properties of seawater: A review of existing correlations and data," *Desalination Water Treat.*, vol. 16, pp. 354–380, Apr. 2010.

[35] C. Marangoni, "Sul principio della viscosita' superficiale dei liquidi stabilito dalsig. *J. Plateau*," *Il Nuovo Cimento*, vol. 5, no. 1, pp. 239–273, 1871.

[36] W. Alpers and H. Hühnerfuss, "The damping of ocean waves by surface films: A new look at an old problem," *J. Geophys. Res., Oceans*, vol. 94, no. C5, pp. 6251–6265, 1989, doi: 10.1029/JC094iC05p06251.

[37] A. D. Jenkins and A. S. Jacobs, "Wave damping by a thin layer of viscous fluid," *Phys. Fluids*, vol. 9, no. 5, pp. 1256–1264, 1997.

[38] P. P. Lombardini, B. Fiscella, P. Trivero, C. Cappa, and W. D. Garrett, "Modulation of the spectra of short gravity waves by sea surface films: Slick detection and characterization with a microwave probe," *J. Atmos. Ocean. Technol.*, vol. 6, no. 6, pp. 882–890, 1989, doi: 10.1175/1520-0426(1989)006<0882:MOTSOS>2.0.CO;2.

[39] K. Folgerø, "Bilinear calibration of coaxial transmission/reflection cells for permittivity measurement of low-loss liquids," *Meas. Sci. Technol.*, vol. 7, no. 9, pp. 1260–1269, 1996.

[40] T. Friisø, Y. Schildberg, O. Rambeau, T. Tjomsland, H. Førdedal, and J. Sjøblom, "Complex permittivity of crude oils and solutions of heavy crude oil fractions," *J. Dispersion Sci. Technol.*, vol. 19, no. 1, pp. 93–126, 1998, doi: 10.1080/01932699808913163.

[41] A. Sihvola, "Electromagnetic mixing formulas and applications," in *Electromagnetic Waves*. Edison, NJ, USA: IET, 1999. [Online]. Available: http://digital-library.theiet.org/content/books/ew/pbew047e

[42] C.-A. Guérin and A. Sentenac, "Separation of surface and volume effects in scattering from heterogeneous rough surfaces: derivation of a splitting rule," *J. Opt. Soc. Amer. A, Opt. Image Sci.*, vol. 24, no. 2, pp. 385–390, Feb. 2007. [Online]. Available: http://josaa.osa.org/abstract.cfm?URI=josaa-24-2-385

[43] T. Elfouhaily and C.-A. Guérin, "A critical survey of approximate scattering wave theories from random rough surfaces," *Waves Random Media*, vol. 14, no. 4, pp. R1–R40, 2004, doi: 10.1088/0959-7174/14/4/R01.

[44] S. O. Rice, "Reflection of electromagnetic waves from slightly rough surfaces," *Commun. Pure Appl. Math.*, vol. 4, nos. 2–3, pp. 351–378, Aug. 1951.

[45] G. R. Valenzuela, "Theories for the interaction of electromagnetic and oceanic waves—A review," *Boundary-Layer Meteorol.*, vol. 13, nos. 1–4, pp. 61–85, 1978.

[46] P. Beckmann and A. Spizzichino, *The Scattering of Electromagnetic Waves from Rough Surfaces*. Norwood, MA, USA: Artech House, 1963.

[47] A. G. Voronovich, "Small-slope approximation in wave scattering from rough surfaces," *J. Exp. Theor. Phys.*, vol. 62, no. 1, pp. 65–70, 1985.

[48] A. G. Voronovich, "Small-slope approximation for electromagnetic wave scattering at a rough interface of two dielectric half-spaces," *Waves Random Media*, vol. 4, no. 3, pp. 337–367, 1994.

[49] A. G. Voronovich, *Wave Scattering from Rough Surfaces*. Berlin, Germany: Springer, 1994.

[50] J. Wright, "A new model for sea clutter," *IEEE Trans. Antennas Propag.*, vol. AP-16, no. 2, pp. 217–223, Mar. 1968.

[51] G. Soriano and C.-A. Guérin, "A cutoff invariant two-scale model in electromagnetic scattering from sea surfaces," *IEEE Geosci. Remote Sens. Lett.*, vol. 5, no. 2, pp. 199–203, Apr. 2008.

[52] B. Chapron, V. Kerbaol, D. Vandemark, and T. Elfouhaily, "Importance of peakedness in sea surface slope measurements and applications," *J. Geophys. Res., Oceans*, vol. 105, no. C7, pp. 17195–17202, 2000, doi: 10.1029/2000JC900079.

[53] T. Elfouhaily, S. Guignard, R. Awadallah, and D. R. Thompson, "Local and non-local curvature approximation: A new asymptotic theory for wave scattering," *Waves Random Media*, vol. 13, no. 4, pp. 321–337, 2003, doi: 10.1088/0959-7174/13/4/308.

[54] C.-A. Guérin, G. Soriano, and T. Elfouhaily, "Weighted curvature approximation: Numerical tests for 2D dielectric surfaces," *Waves Random Media*, vol. 14, no. 3, pp. 349–363, 2004, doi: 10.1088/0959-7174/14/3/009.

[55] A. A. Mouche, B. Chapron, and N. Reul, "A simplified asymptotic theory for ocean surface electromagnetic wave scattering," *Waves Random Complex Media*, vol. 17, no. 3, pp. 321–341, 2007, doi: 10.1080/17455030701230261.

[56] A. A. Mouche, B. Chapron, N. Reul, D. Hauser, and Y. Quilfen, "Importance of the sea surface curvature to interpret the normalized radar cross section," *J. Geophys. Res., Oceans*, vol. 112, no. C10, 2007, doi: 10.1029/2006JC004010.

[57] C.-A. Guérin, G. Soriano, and B. Chapron, "The weighted curvature approximation in scattering from sea surfaces," *Waves Random Complex Media*, vol. 20, no. 3, pp. 364–384, 2010.

[58] G. Caulliez and C.-A. Guérin, "Higher-order statistical analysis of short wind wave fields," *J. Geophys. Research: Oceans*, vol. 117, no. C6, 2012, doi: 10.1029/2011JC007854.

[59] S. Angelliaume, X. Ceamanos, F. Viallefont-Robinet, R. Baqué, P. Déliot, and V. Miegebielle, "Hyperspectral and radar airborne imagery over controlled release of oil at sea," *Sensors*, vol. 17, no. 8, p. 1772, 2017. [Online]. Available: http://www.mdpi.com/1424-8220/17/8/177

[60] M. Gade, W. Alpers, H. Hühnerfuss, H. Masuko, and T. Kobayashi, "Imaging of biogenic and anthropogenic ocean surface films by the multifrequency/multipolarization SIR-C/X-SAR," *J. Geophys. Res., Oceans*, vol. 103, no. C9, pp. 18851–18866, 1998, doi: 10.1029/97JC01915.

[61] W. Alpers, B. Holt, and K. Zeng, "Oil spill detection by imaging radars: Challenges and pitfalls," *Remote Sens. Environ.*, vol. 201, pp. 133–147, Nov. 2017. [Online]. Available: http://www.sciencedirect.com/science/article/pii/S0034425717304145

[62] *MOS Sweeper—Egersund Group*. Accessed: Oct. 23, 2017. [Online]. Available: http://www.egersundgroup.no/oilspill/mos-sweeper-

[63] I. Hajnsek, E. Pottier, and S. R. Cloude, "Inversion of surface parameters from polarimetric SAR," *IEEE Trans. Geosci. Remote Sens.*, vol. 41, no. 4, pp. 727–744, Apr. 2003.

[64] Z. Guerraou, "Rétrodiffusion micro-onde par la surface océanique en incidence élevée: Approche conjointe expérimentale et théorique," (in French), Ph.D. dissertation, Univ. Toulon, Toulon France, Sep. 2017.

Olivier Boisot received the M.S. degree in physics and engineering sciences and the Ph.D. degree in physics, with a focus on ocean remote sensing, from the University of Toulon, La Garde, France, in 2012 and 2015, respectively.

He was a Post-Doctoral Fellow with the Electromagnetism and Radar Department, Office National d'Études et de Recherches Aérospatiales (ONERA), Salon-de-Provence, France, where he was involved in the marine oil slicks quantification from synthetic aperture radar (SAR) measurements in microwave bands. He is currently with ONERA, where he is involved in SAR interferometry capabilities over the ocean surface.

Sébastien Angelliaume received the master's degree in engineering from the École Nationale Supérieure d'Ingénieur de Constructions Aéronautiques, Toulouse, France, in 2003, and the M.S. degree from the École Nationale Supérieure d'Électrotechnique, d'Électronique, d'Informatique, d'Hydraulique et des Télécommunications, Toulouse, in 2003.

Since 2006, he has been with the Electromagnetism and Radar Department, Office National d'Études et de Recherches Aérospatiales (ONERA—The French Aerospace Laboratory), Salon-de-Provence, France. He has been involved in the ONERA synthetic aperture radar airborne platforms RAMSES and SETHI, developing science applications. Since 2010, his research at ONERA focuses mainly on remote sensing over the ocean surface.

Charles-Antoine Guérin received the B.Eng. degree from the École Nationale Supérieure de l'Aéronautique et de l'Espace, Toulouse, France, in 1994, and the Ph.D. degree in theoretical physics from the University of Aix-Marseille, Marseille, France, in 1998.

He is currently a Professor and a Researcher with the Mediterranean Institute of Oceanography, University of Toulon, Toulon, France, where he is involved in ocean remote sensing.